Journal of Fluids and Structures (1997) **11,** 293–305

DYNAMICS AND FORCING OF A TETHERED SPHERE IN A FLUID FLOW

C. H. K. WILLIAMSON AND R. GOVARDHAN
Mechanical & Aerospace Engineering, Upson Hall
Cornell University, Ithaca, NY 14853, U.S.A.

(Received 26 January 1996 and in revised form 18 November 1996)

Despite the practical significance of studying the case of the tethered sphere in a steady flow, there are almost no laboratory investigations for such a problem, and it was previously unknown whether such a system would tend to oscillate or not. It is also common ocean engineering practice to assume no oscillation effects in predictions of drag and tether angle of a tethered body. The present work demonstrates that a tethered sphere will oscillate remarkably vigorously at a saturation amplitude of close to two diameters peak-to-peak. The oscillations induce an increase in drag and tether angle of the order of around 100% over what is predicted using nonoscillating drag measurements. Analysis of in-line and transverse natural frequencies indicate that these frequencies should have the same value. Our experiments show that the in-line oscillations become phase locked with the transverse oscillations and vibrate at *twice* the frequency of the transverse motion. The above results suggest that oscillations are highly significant to predictions of sphere response in a steady flow, and should not be neglected. Finally, although response amplitudes show large disparity when plotted against Reynolds number, under a range of different sphere mass ratios (M^*) and tether length ratios (L^*), we find an excellent collapse of data for the different experiments by plotting the amplitudes versus the reduced velocity $V_R = U/f_n D$. This result shows that, for very small structural damping, the response amplitude may be considered as a function of the (normalized) natural frequency, and is only a function of the mass ratio and length ratio in so much as these parameters influence the natural frequency itself.

© 1997 Academic Press Limited

1. INTRODUCTION

PERHAPS ONE OF THE MOST BASIC of fluid–structure interactions that one can imagine is a tethered sphere (or bluff body) in a fluid flow. By a wide variation of the mass ratio of the sphere, one can consider the case of an underwater tethered buoyant body, or a heavy sphere "pendulum" in air flow, as examples of essentially the same general problem. Typical predictions, employed by practising ocean engineers, of tether angle θ and mean drag coefficient C_D (see Figure 1) for a tethered buoyant sphere in a current, involve using the well-established sphere drag data in the literature [for example, Wieselsberger (1922) to be found in Schlichting (1979)]. It is highly surprising that, despite the fact that tethered bodies are quite ubiquitous in engineering, no investigations have shown precisely whether a tethered sphere will oscillate in a steady fluid flow or current. In the present work, we demonstrate that such a structure will indeed vibrate vigorously, and these oscillations have a direct impact on the tether angle and drag coefficient. Gross errors in predictions of mean response of tethered structure will ensue unless one takes account of their tendency to vibrate.

Previous studies in the literature concerning a tethered sphere in a fluid flow appear to be concerned primarily with the action of surface waves on tethered buoyant

0889–9746/97/030293 + 13 $25.00/fl960078 © 1997 Academic Press Limited

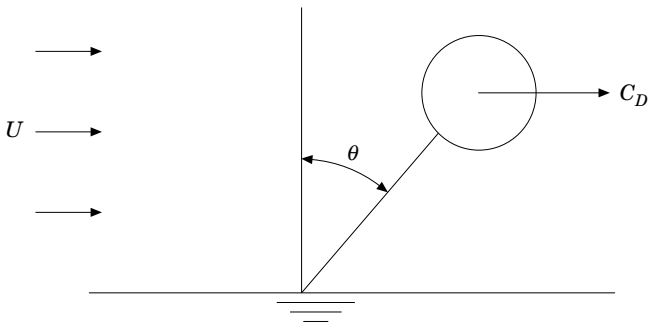

Figure 1. Idealized sketch of a tethered sphere in fluid flow. The tethered sphere is inclined at an angle (θ), relative to the vertical, due to the drag force on the sphere.

structures (Harleman & Shapiro 1961; Shi-Igai & Kono 1969; Ogihara 1980; Vethamony *et al.* 1992; Carpenter *et al.* 1995). As in the case of the prediction of flow-induced vibrations for a cylinder in waves, most of these investigations employ empirically determined drag and inertia coefficients of the type used originally for fixed structures in "Morison's" equation. As may be expected, the combination of wave motions and dynamics of the tethered bodies yield highly complicated equations of motion, from which it is rather difficult to understand any of the underlying physics. It is also clear that a tethered body will indeed vibrate in such a wave field, simply because of the harmonic oscillations of the fluid velocity past the structure. Mention must also be made of the work of Mei (1994) on an oscillating sphere at low Reynolds number, Howe (1995) on forces on a sphere at low Reynolds number, Otto (1992) on an oscillating sphere in still water and Tsuji *et al.* (1991) on the forces on a sphere in a pulsed flow, although they are not directly relevant to the present work. In the present, conceptually simple, case of a tethered sphere in a current, we have found no published work whatsoever which investigates the propensity of the tethered structure to vibrate. It is to this problem that we address ourselves in this study. Of significance are the frequencies of the fluid-induced vibrations, and their relation to the natural system frequency, and to the vortex formation frequency in the wake of a sphere. We are particularly interested in a study of the wake vortical motions giving rise to any such vibrations. In the present work, we shall show a remarkable propensity for the sphere to vibrate, and will demonstrate the significant effect of these oscillations on the drag and tether angle, which is clearly of practical significance in itself. However, our presented results constitute the first phase of our investigations, and the vortex dynamics and a study of the frequency of oscillations will be included elsewhere. It appears that the large scatter in previous measurements of Strouhal frequency for a fixed sphere (shown in Figure 7) leads to difficulties in precise conclusions about the synchronization of the sphere motion, and further careful Strouhal frequency measurements are required.

2. EXPERIMENTAL METHOD

Our experiments have been performed in the Cornell-ONR Water Channel, which has a cross-section of 15 in. by 20 in., and a maximum speed of 35 cm/s. The turbulence level is 0·9% and flow uniformity is better than 1·5% over 80% of the channel width. To achieve an accurate determination of fluid velocity through the channel, we have utilized a DISA Laser Doppler anemometer in the forward scattering mode. The

spheres are of diameter 3·92 cm and 3·77 cm, and weigh 23 and 2·3 g respectively. We chose these parameters in order to yield a wide variation in the sphere mass, which is characterized in terms of a mass ratio, M^*, where

$$M^* = \frac{\text{sphere mass}}{\text{displaced mass of fluid}} = \frac{M}{\frac{1}{6}\pi D^3 \rho}. \tag{1}$$

The "high-mass" sphere corresponds with $M^* = 0{\cdot}73$, while the "low-mass" sphere has $M^* = 0{\cdot}082$. The spheres are tethered, using thin line (gut), to the floor of the water channel. The tether length of the spheres was such as to keep the bodies always submerged.

One can imagine that determining the position of the sphere as a function of time must be achieved nonintrusively, since any extra lines attached to the sphere would undoubtedly affect the dynamic response. Our technique to find $X(t)$ and $Y(t)$, which are the in-line and transverse sphere displacements, involves image processing every single video image taken of the sphere motion, over a large number of cycles. This is very time-intensive, although it is *essential* to yield the time variation and spectra of the x and y oscillations. The sphere oscillations are recorded by a S-VHS Video recorder, through a CCD camera placed vertically under the test section, as shown schematically in Figure 2(a). The sphere displacements are analysed with image-processing hardware installed on a 486-computer. The computer is programmed to control the VCR, in a fully automatic process, utilizing accurate time position of each frame, incorporating the time code written on the audio track of the tape. The position of the sphere in each frame is determined using a simple geometric approach, where the outline of the edge of the dark sphere against a lighter background (for the camera viewing upwards) is found, and thereby the centre of the sphere is deduced, as indicated in the example picture of the video screen in Figure 2(b). With a video framing rate of 30 Hz, and a typical sphere oscillation of around 0·5–2·5 Hz, we find sufficient resolution by analysing every video frame. The tether angle is calculated by determining the mean streamwise displacement of the sphere from the undisturbed position, taking into account the effects of parallax.

3. LARGE VIBRATIONS AND FLUID LOADING OF A TETHERED SPHERE

Initially, we simply set up the very light sphere of low mass ratio, ($M^* = 0{\cdot}082$) tethered to the floor of our water channel, and we immediately observed wild oscillations of the tethered sphere at almost all the flow speeds investigated. This gave us an early indication that fluid-induced oscillations, which are generally ignored in engineering predictions for this problem, would be significant.

Predictions of the natural frequencies in the X and Y-directions can be made as follows. Taking account of drag force, buoyancy, weight and tether tension, both the in-line and transverse frequencies are given by the same equation,

$$f_n = \frac{1}{2\pi}\sqrt{\frac{T}{M}}. \tag{2}$$

The normalized natural frequency may be written in terms of a "Strouhal" number, S_n,

$$S_n = \frac{f_n D}{U} = \left(\frac{\sqrt{3}}{4\pi}\right)\sqrt{\frac{C_T}{(M^* + C_a)L^*}}, \tag{3}$$

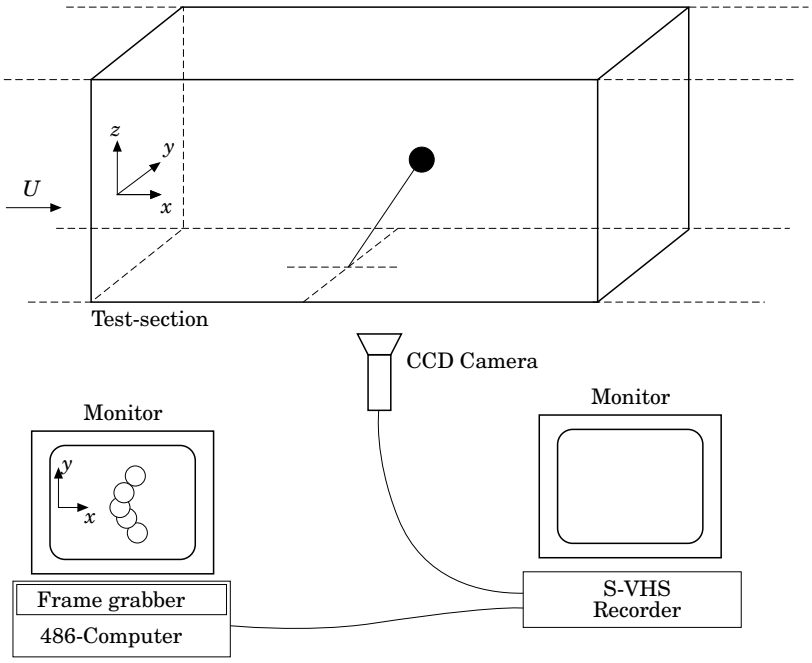

(a)

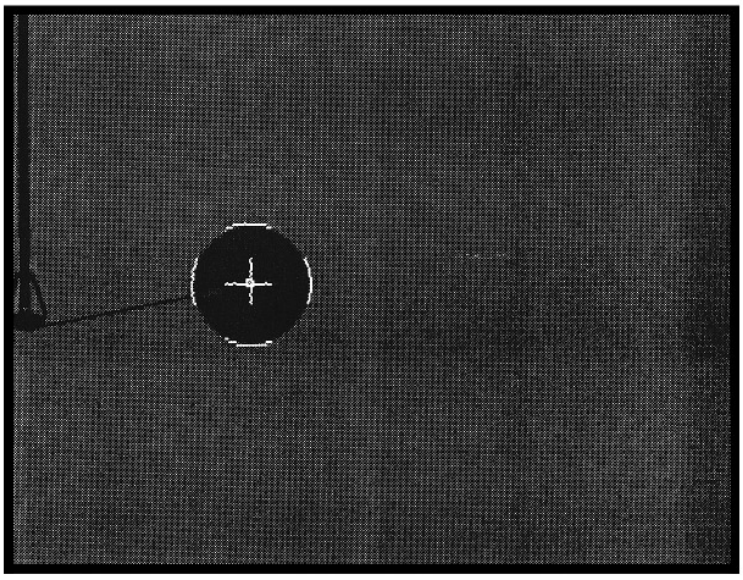

(b)

Figure 2. (a) Experimental image processing arrangement for determining sphere position. (b) Sample image of analyzed video frame, showing determination of sphere position.

where the tension coefficient is given by

$$C_T = \frac{T}{0{\cdot}5\rho U^2(\pi D^2/4)} = \left[C_D^2 + \frac{16}{9}\frac{(1-M^*)^2}{\mathrm{Fr}^4}\right]^{1/2}, \tag{4}$$

and C_a = added mass coefficient = 0·5, L^* = tether length/diameter = L/D, Fr = Froude number = $U/\sqrt{gD}$.

We can estimate the relative magnitude of the two terms in the tension coefficient. In both the laboratory and in the ocean, we take a typical mass ratio, $M^* = 0{\cdot}5$. In the ocean, we take a typical spherical buoyant object as around 2 m diameter, in a current of, say, 2 m/s, whereas typical values in the laboratory are 0·05 m diameter in a current of 0·1 m/s. These values yield Froude numbers of 0·45 in the ocean versus 0·14 in the laboratory. In the ocean, the first term in the tension coefficient is of the order of 2% of the second term, whereas in the laboratory, the first term is around 0·02% of the second term. We may thus neglect, in many cases of interest, the C_D^2 term in (4), to give

$$S_n \approx \left(\frac{1}{2\pi}\right) \frac{1}{\mathrm{Fr}\sqrt{L^*}} \sqrt{\frac{1 - M^*}{C_a + M^*}}. \tag{5}$$

These simple predictions for the natural frequency of oscillation are of the same order as those we observe, although, as stated earlier, precise conclusions regarding synchronization of the sphere oscillations with the vortex formation frequency in the wake of the sphere require further accurate determination of Strouhal frequencies, due to the large scatter presently in the literature. However, it is of interest that the above equation for the natural frequency applies to both the in-line and transverse oscillations; the two natural frequencies are the same. We present, in Figure 3, profiles of the transverse Y-oscillations and in-line X-oscillations for around Re = 5100, and for the low-mass sphere ($M^* = 0{\cdot}082$), where it is immediately seen that the actual sphere fluid-induced vibrations are quite different. The in-line vibrations are at *twice* the frequency of the transverse vibrations. One might expect this 2:1 ratio of frequencies based on physical grounds, since the conditions affecting in-line vibrations when the sphere is displaced to $+Y$, will be just the same as when the sphere is displaced to $-Y$. This is similar to the fact that the in-line drag force on a cylinder is at twice the frequency of the lift force due to the alternate vortex shedding. The x-y displacement pattern, or phase plot, in Figure 3(c) shows a typical characteristic pattern.

As we increase Reynolds number to around Re = 9200, in Figure 4, we find that the sphere oscillations build up to an amplitude of around $0{\cdot}4D$ in the transverse direction, and around half of this value in the in-line direction, and again, the in-line vibrations are at twice the frequency of the transverse oscillations. The phase between the X and Y motions changes, as Re is increased to Re = 9200 as shown in Figure 4(c). For further increases in Re to around Re = 11 300, in Figure 5, the transverse oscillations build up to $0{\cdot}6D$, whereas the in-line vibrations have reached a saturation amplitude of around $0{\cdot}2D$. The phase plot is further changing to become a "figure-of-eight" shape. The vibration spectra of Figure 6 show clearly that the in-line oscillations are at *twice* the frequency of the transverse oscillations. A full understanding of this 2:1 frequency ratio, as well as an understanding of the fluid forcing causing the large oscillation amplitudes and phase plots requires an investigation into the wake vortex dynamics, which project we shall soon embark upon. However, it is important in a practical sense, that we have discovered that a tethered sphere will vibrate, and indeed in a vigorous manner, and further that the frequency of the in-line oscillations is twice that frequency for transverse vibration, contrary to predictions. Both of these phenomena will be found to be highly significant to the drag and tether angle, which are rather basic parameters for such a tethered system.

From the preceding paragraph it is seen that the response amplitude is a function of the flow velocity. We prefer initially to use the Reynolds number to characterize the flow velocity as it is not known, ahead of time, that the flow field is necessarily independent of Reynolds number in the Reynolds number range of our experiments.

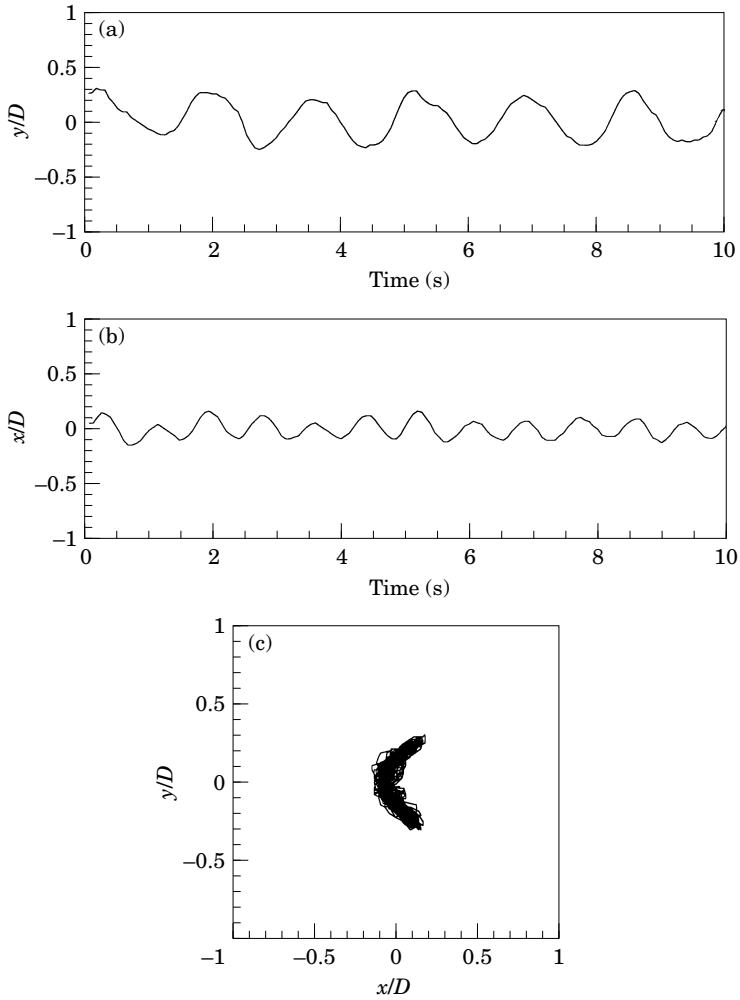

Figure 3. Time traces of (a) transverse (y) oscillations, (b) streamwise (x) oscillations of the tethered sphere, and (c) the x-y phase plot of the oscillations. Reynolds number Re = 5132, the mass ratio $M^* = 0{\cdot}082$ and the normalized tether length $L^* = 9{\cdot}3$.

This is apparent from the several measurements in the literature for Strouhal number (for a fixed sphere) versus Reynolds number, shown in Figure 7, where there is some distinct variation over the range of Reynolds number used here. However, we shall later demonstrate a reasonable collapse of response data when plotting versus the (classical) reduced velocity parameter, $V_R = U/f_n D$.

Response amplitudes for the low-M^* sphere, over a wide range of Reynolds number, Re, are given in Figure 8(a). Over the whole range of Re (up to 13 000), the amplitude of transverse oscillation appears to be increasing. On the other hand, over the same range of Re in Figure 8(b), a high-M^* sphere ($M^* = 8{\cdot}93$) indicates similarly that there is a gradual increase of vibration amplitude, but it appears to reach a saturation amplitude at Re = 5000, and to continue at the same level of about two diameters peak-to-peak up to the highest Re investigated. The responses of the two systems seem to be quite different. The saturation in-line oscillation amplitude reaches a value of around $0{\cdot}2D$ for the low-mass sphere, and a value of $0{\cdot}1D$ for the high-mass sphere.

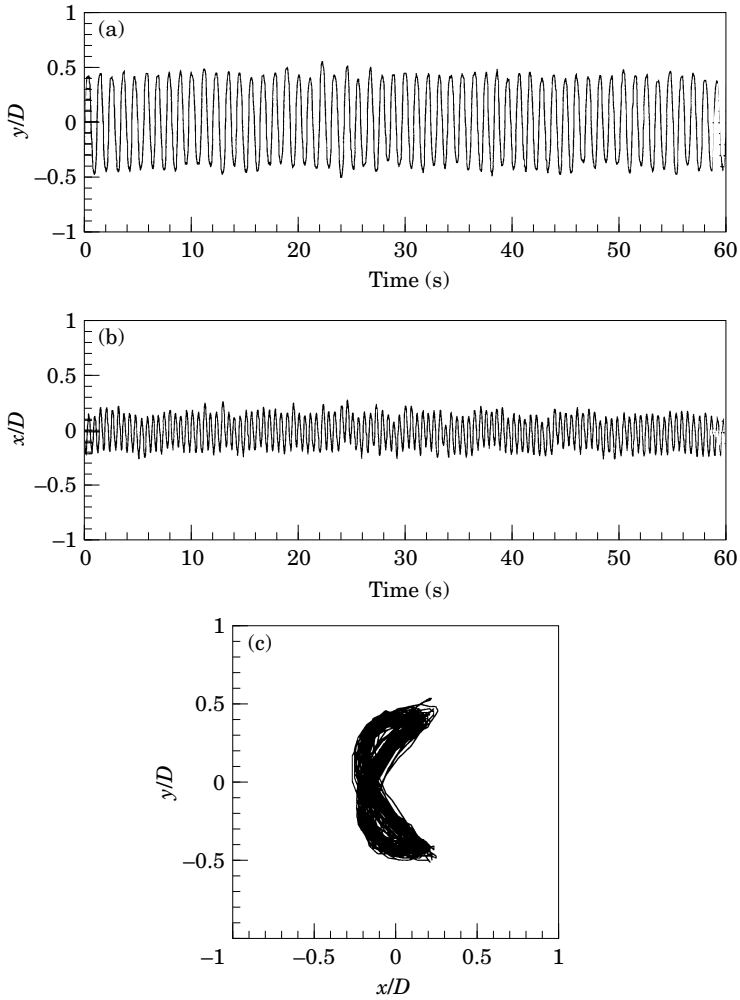

Figure 4. Time traces of (a) transverse (y) oscillations, (b) streamwise (x) oscillations of the tethered sphere and (c) the x-y phase plot of the oscillations. Reynolds number Re = 9176, the mass ratio $M^* = 0{\cdot}082$ and the normalized tether length $L^* = 9{\cdot}3$.

We have also investigated the effect of changing the tether length L^*. The value of L^* for the preceding cases is around 9, and for the high-mass sphere, we also studied the case of $L^* = 3{\cdot}8$ [see Figure 8(c)]. It is of great interest that this does not appear to affect either the saturation amplitudes in the transverse or in-line directions! The major difference is a shift of the Reynolds number where the oscillating system reaches its maximum amplitude, in this case saturating at Re around 8000. The similarities in the increasing segments of the response plots, for all three cases above, suggests that similar phenomena may be occurring for the three cases, but at shifted Re values, and perhaps there exists a more suitable parameter with which to scale the data. We investigate this point below.

Dimensional analysis shows that, if the response amplitude depends on the following variables:

$$A/D = \{f_n, M, \rho, U, L, g, \mu\}, \tag{6}$$

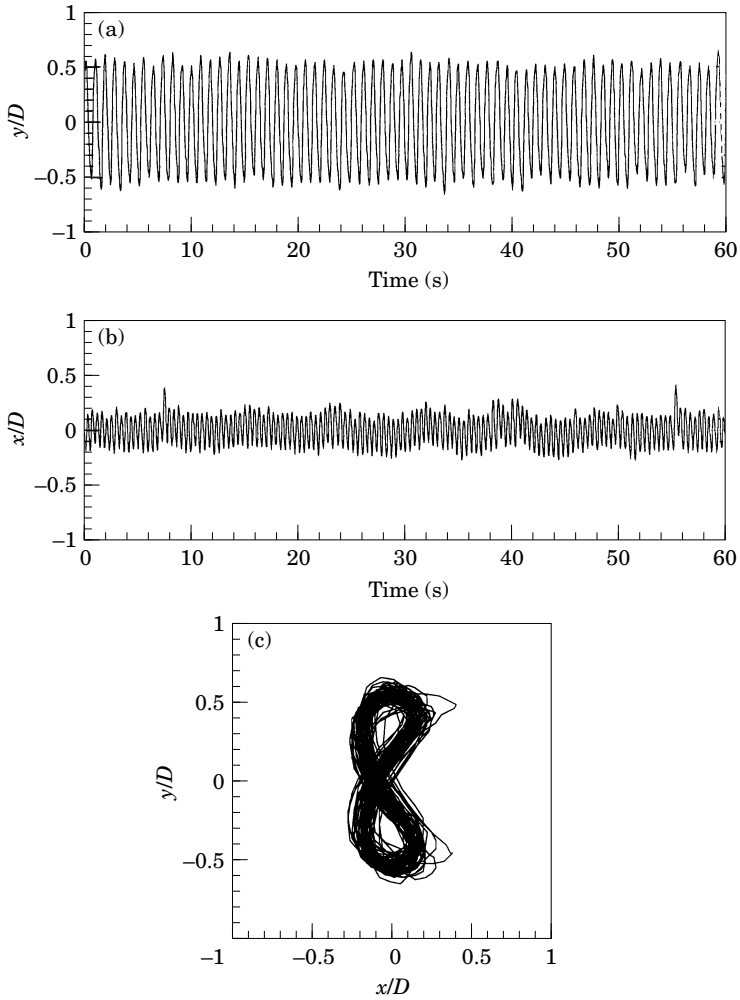

Figure 5. Time traces of (a) transverse (y) oscillations, (b) streamwise (x) oscillations of the tethered sphere and (c) the x-y phase plot of the oscillations. Reynolds number Re = 11 310, the mass ratio $M^* = 0{\cdot}082$ and the normalized tether length $L^* = 9{\cdot}3$.

where ρ and μ are the fluid density and viscosity, then one may deduce the following nondimensional groups;

$$A/D = \text{function}\{M^*,\ V_R,\ L^*,\ \text{Fr},\ \text{Re}\}, \tag{7}$$

where $V_R = \text{reduced velocity} = U/f_n D$. One could suggest that the parameters $\{M^*, L^*, \text{Fr}\}$ serve to change the particular value of the natural frequency that most directly influences the response shape (but perhaps not necessarily the saturation amplitude). Let us now make the assumption that the fluid forcing is essentially independent of Reynolds number, since the effects of viscosity are mainly to set the boundary layer thickness at separation, with essentially inviscid vorticity dynamics thereafter in the near wake, then one has the simpler relation:

$$A/D = \text{function}\{V_R\}. \tag{8}$$

In essence, we make the assumption that, although Reynolds number has some effect

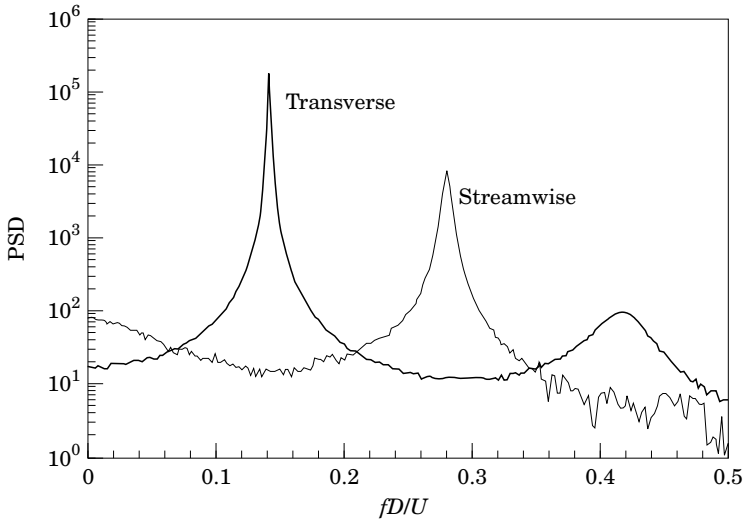

Figure 6. Spectra of streamwise (x) and transverse (y) oscillations of the tethered sphere, showing clearly that the streamwise oscillation frequency is twice the transverse oscillation frequency. Reynolds number Re = 11 310, the mass ratio $M^* = 0{\cdot}082$ and the normalized tether length $L^* = 9{\cdot}3$.

on vortex formation for a *fixed sphere* over the relevant Reynolds number range, the case of an *oscillating sphere* could nevertheless be independent of Reynolds number. This assumption, which is by no means an obvious point, can be checked by the results we now present. If we replot the three sets of response data from Figures 8(a–c) in a single plot shown in Figure 9, we find an excellent collapse of the normalized amplitude with this single shown in Figure 9, we find an excellent collapse of the normalized amplitude with this single parameter, the reduced velocity $V_R = U/f_nD$, and is reasonably independent of the mass ratio M^* or tether length ratio L^*, except insofar

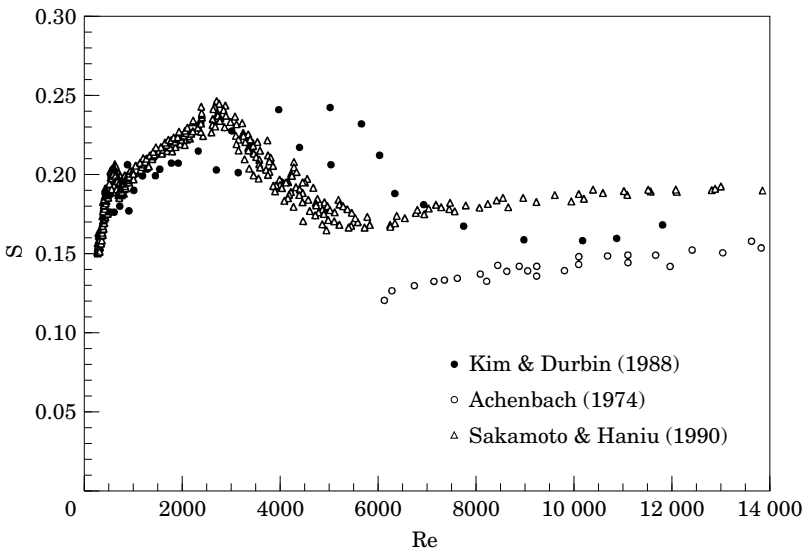

Figure 7. Variation of Strouhal number (S) versus Reynolds number (Re), for flow past a rigidly held sphere, from previous measurements.

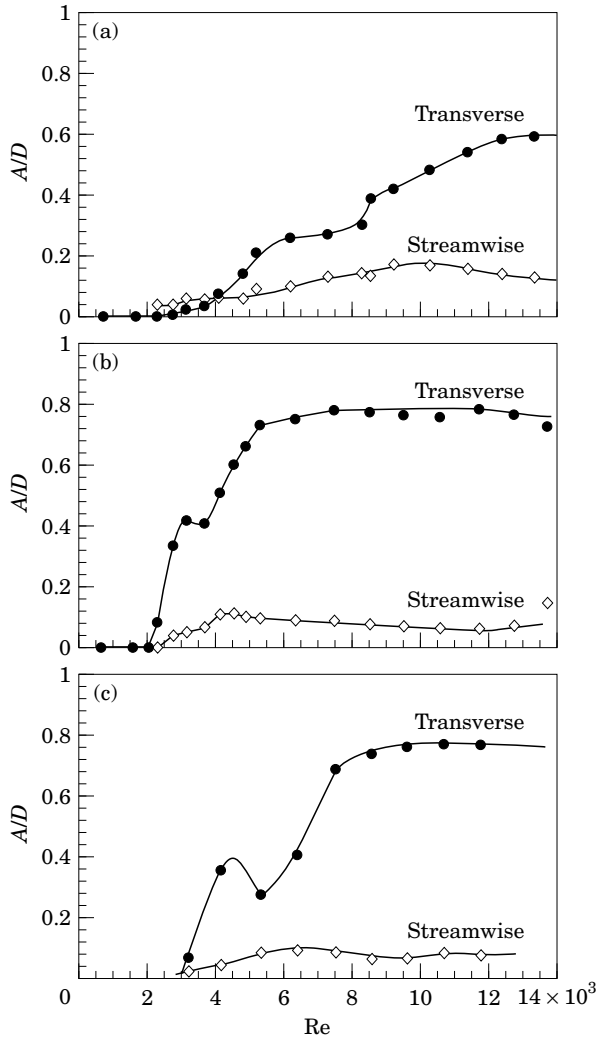

Figure 8. Normalized oscillation amplitude (A/D) versus Reynolds number (Re) for (a) low mass ratio case ($M^* = 0{\cdot}082$) and $L^* = 9{\cdot}3$, (b) high mass ratio case ($M^* = 0{\cdot}73$) and $L^* = 8{\cdot}9$, (c) high mass ratio case ($M^* = 0{\cdot}73$) and $L^* = 3{\cdot}8$.

as these groups influence the value of f_n. This would appear to be a useful practical result for tethered ocean engineering structures.

Mention must also be made of the small (first) local maximum in response amplitude which seems to appear in all amplitude plots of Figure 8(a–c), when the amplitude data is increasing. In the collapsed data plot of Figure 9, we can see that this maximum is around $U/f_nD = 5$ to 6, and this corresponds roughly to the inverse of the Strouhal number of a fixed-sphere vortex shedding (see Figure 7). Under these conditions, the natural frequency is approximately equal to the vortex formation frequency, and it is this condition that yields a resonance in classical studies of flow-induced vibration for cylinders. It is clear that the sphere response, although exhibiting some maximum for this resonance condition, has a shape for the larger broad saturation amplitude (at higher V_R) which is quite distinct from the well known cylinder-oscillation problem.

The existence of large vibrations of a tethered structure causes a significant

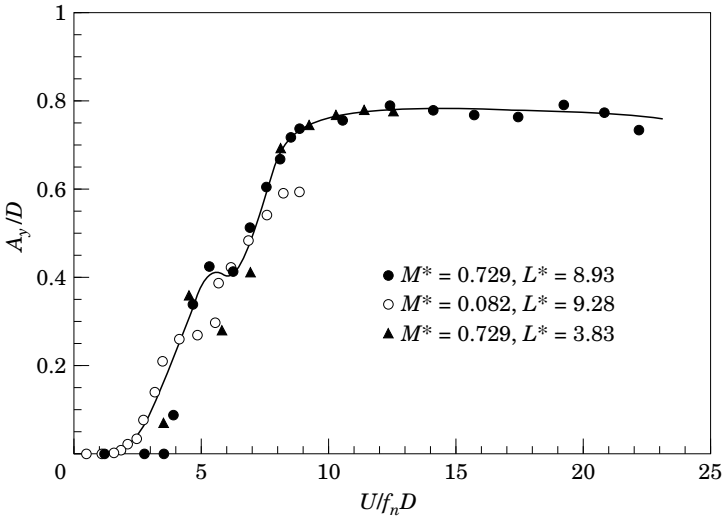

Figure 9. Normalized transverse oscillation amplitude (A_y/D) versus reduced velocity (U/f_nD), showing collapse of data for different mass ratios (M^*) and normalized tether lengths (L^*).

amplification in the drag coefficient of the order of 100% over the values measured originally by Weiselsberger (1922) and plotted in Schlichting (1979), as demonstrated in Figure 10(a). The mean drag may be related to the mean angle of inclination of the tethered sphere by considering the tension of the tether and the buoyancy force, as follows:

$$\tan\theta = (\tfrac{3}{4})\frac{\mathrm{Fr}^2 C_D}{1 - M^*}. \tag{9}$$

Correspondingly, the transverse oscillations also cause roughly a 100% increase in the angle of inclination θ of such a tethered body in a current, over the values predicted using nonoscillating drag coefficients, as shown in Figure 10(b).

4. CONCLUDING REMARKS

It appears quite surprising that almost no studies have been directed towards the dynamics of tethered spheres in a steady fluid flow, and that it was previously unknown whether such a system would tend to oscillate or not. It is also common ocean engineering practice to assume no oscillation effects in predictions of drag and tether angle of a tethered body. The present work demonstrates that a tethered sphere will oscillate remarkably vigorously at a saturation amplitude of close to two diameters peak-to-peak. The oscillations induce an increase in drag and tether angle of around 100% over what is predicted using nonoscillating drag measurements. Analysis of in-line and transverse natural frequencies indicate that these frequencies should have the same value. Our experiments show that the in-line oscillations become phase locked with the transverse oscillations and vibrate at *twice* the frequency of the transverse motion. The above results suggest that oscillations are highly significant to predictions of sphere response in a steady flow, and should not be neglected.

Although we have discovered large oscillations in a tethered sphere system and the corresponding magnification of the fluid loading on the system, which have immediate practical application, further research on this problem is necessary. We must understand the relation of the fluid-induced vibration frequency to the natural

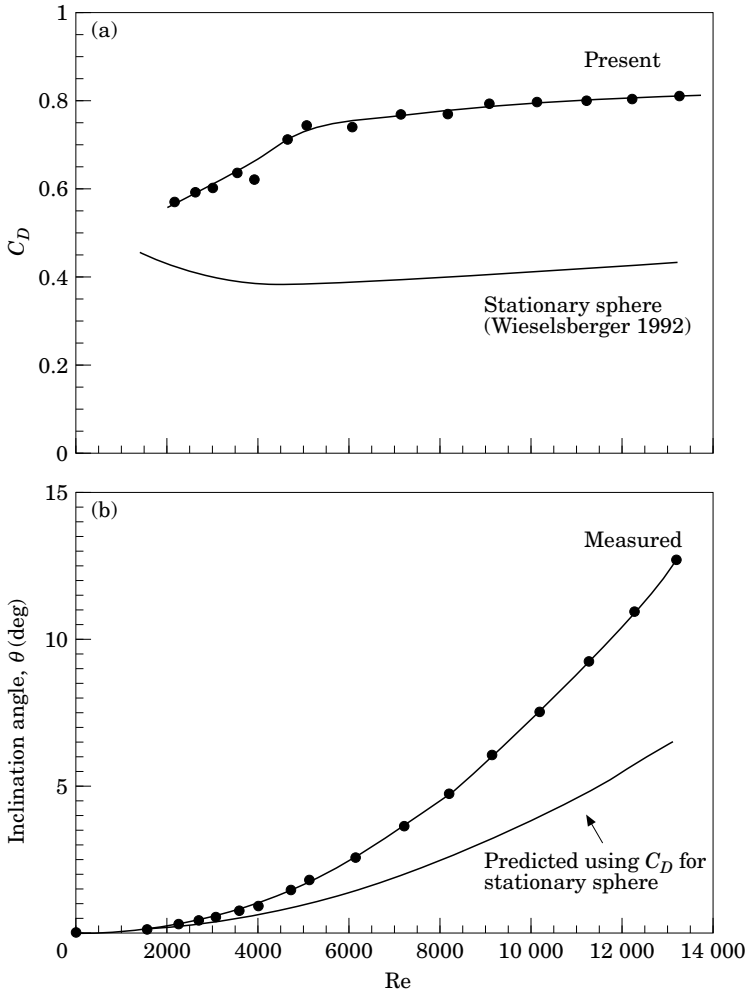

Figure 10. Amplification of (a) drag and (b) tether angle due to sphere oscillations. $M^* = 0{\cdot}082$, $L^* = 9{\cdot}3$.

frequency and to the vortex formation frequency. Although one can compute the natural frequency using the simple equations derived in this paper, we can see that there is a large scatter amongst the measurements of vortex formation frequency in the wake of a sphere, as demonstrated by Figure 7. We are therefore embarking on a measurement of Strouhal frequency for a fixed sphere to make precise conclusions regarding the synchronization between natural and vortex-shedding frequencies. It is also clear that an understanding of the wake vortex dynamics is needed, which will also aid in interpreting the response phenomena, and we intend to conduct flow visualization as well as Digital Particle Image Velocimetry (DPIV) on this problem.

ACKNOWLEDGEMENTS

The support from the Ocean Engineering Division of the O.N.R., monitored by Tom Swean, is gratefully acknowledged (O.N.R. Contract No. N00014-94-1-1197 and N00013-95-1-0332).

References

Achenbach, E. 1974 Vortex shedding from spheres. *Journal of Fluid Mechanics* **62,** 209–221.

Carpenter, E. B., Leonard, J. W. & Yim, S. C. S. 1995 Experimental and numerical investigations of tethered spar and sphere buoys in irregular waves. *Ocean Engineering* **22,** 765–784.

Harleman, D. R. F. & Shapiro, W. C. 1961 The dynamics of a submerged moor sphere in oscillatory waves. *Coastal Engineering* **2,** 746–765.

Howe, M. S. 1995 On the force and moment on a body in an incompressible fluid, with applications to rigid bodies and bubbles at high and low Reynolds number. *Quarterly Journal of Mechanics & Applied Mathematics* **48,** 401–426.

Kim, K. J. & Durbin, P. A. 1988 Observation of the frequencies in a sphere wake and drag increase by acoustic excitation. *Physics of Fluids* **31,** 3260–3265.

Mei, R. 1994 Flow due to an oscillating sphere and an expression for unsteady drag on the sphere at finite Reynolds number. *Journal of Fluid Mechanics* **270,** 133–174.

Ogihara, K. 1980 Theoretical analysis on the transverse motion of a buoy by a surface wave. *Applied Ocean Research* **2,** 51–56.

Otto, S. R. 1992 On stability of the flow around an oscillating sphere. *Journal of Fluid Mechanics* **239,** 47–63.

Sakamoto, H. & Haniu, H. 1990 A study on vortex shedding from spheres in a uniform flow. *ASME Journal of Fluids Engineering* **112,** 386–392.

Schlichting, H. 1979 *Boundary Layer Theory,* Seventh edition, New York: McGraw-Hill.

Shi-igai, H. & Kono, T. 1969 Study on vibration of submerged spheres caused by surface waves. *Coastal Engineering in Japan* **12,** 29–40.

Tsuji, Y., Kato, N. & Tanaka, T. 1991 Experiments on the unsteady drag and wake of a sphere at high Reynolds numbers. *International Journal of Multiphase Flow* **17,** 343–354.

Vethamony, P., Chandramohan, P. & Sastry, J. S. 1992 Estimation of added-mass and damping coefficients of a tethered spherical float using potential flow theory. *Ocean Engineering* **19,** 427–436.

Wieselsberger, C. von 1922 Weitere Festellungen über dei Geset des Flussigkeits und Luftwiderstandes. *Physikalische Zeitschrift* **23,** 219–224.